Studia Geophysica et Geodaetica, manuscript No.
(will be inserted by the editor)

Reflection and transmission coefficients of a fracture in transversely isotropic media

Short title: Fracture scattering in anisotropic media.

José M. Carcione [1] · **Stefano Picotti**[1]

Received: date / Accepted: date

Abstract We obtain the reflection and transmission coefficient of a fracture in transversely isotropic media, whose symmetry axes are perpendicular to the fracture surface. We consider dissimilar upper and lower media. The fracture is modeled as boundary discontinuities in the displacement u and the particle velocity v, of the stresses as $[\kappa u + \eta v]$, where the brackets denote discontinuities across the interface. The specific stiffness κ introduces frequency-dependence and phase changes in the interface response and the specific viscosity η is related to the energy loss. We also calculate the energy balance at the interface and the dissipated energy. The theory is illustrated by computing the reflection coefficient of a fracture present in the Antarctic ice cap. In this case, the reflection coefficient decreases with increasing incidence angle and then approaches 1 at grazing angle.

Keywords Fracture · anisotropy · reflection coefficient · boundary condition · attenuation.

1 Introduction

The study of fracture scattering (reflection-transmission) plays an important role in seismology, exploration geophysics and material science: fractures and cracks in the Earth's crust may constitute possible sources of earthquakes (Pyrak-Nolte et al., 1990), and hydrocarbon and geothermal reservoirs are mainly composed of fractured rocks (Nakagawa and Myer, 2009); moreover, ultrasonic waves are used to detect flaws and cracks in order to prevent material failure (Nagy and Adler, 1990).

Simulation of fracture scattering requires a suitable interface model for describing the dynamic response of the crack surface. Theories that consider imperfect contact were mainly based on the displacement discontinuity model at the interface. Pyrak-Nolte et al. (1990) proposed a non-welded interface model based on the discontinuity of

[1] Istituto Nazionale di Oceanografia e di Geofisica Sperimentale (OGS), Borgo Grotta Gigante 42c, 34010 Sgonico, Trieste, Italy.
E-mail: jcarcione@inogs.it

the displacement and the particle velocity across the interface. The stress components are proportional to the displacement and velocity discontinuities through the specific stiffnesses and one specific viscosity, respectively. Displacement discontinuities conserve energy and yield frequency dependent reflection and transmission coefficients. On the other hand, velocity discontinuities generate an energy loss at the interface. The specific viscosity accounts for the presence of a liquid under saturated conditions. The liquid introduces a viscous coupling between the two surfaces of the fracture (Schoenberg, 1980) and enhances energy transmission, but at the same time this is reduced by viscous losses. The model may account for some slip and dilatancy effects as those described, for instance, by the interface model proposed by Mroz and Giambianco (1996).

The scattering problem in isotropic media has been solved by Carcione (1996, 2007) and Carcione (1998) obtained the normal-incidence reflection and transmission coefficients of a fracture embedded in a homogeneous transversely isotropic (TI) medium. In both cases, numerical simulation were performed by using a pseudospectral method. Elastic wave scattering by a circular crack in a TI solid solid was investigated by Kundu and Boström (1992). They used an analytical solution method and considered stress-free boundary conditions at the interface, implying a complete decoupling of the two surfaces which corresponds to zero stiffnesses and zero specific viscosity. Chiasri and Krebes (2000) obtained the same expressions of Carcione (1996) in the particular case when there is no energy loss.

In this work, we obtain the reflection and transmission coefficients for all angles of incidence by considering displacement and particle-velocity discontinuities at the interface of the fracture embedded in a TI medium. The imperfect bonding is described by four parameters: the normal and tangential specific stiffnesses and viscosities. In order to model a fracture embedded in a finely laminated background, we assume that this is described by a TI medium whose symmetry axis is perpendicular to the fracture surface. For instance, composite materials, or geological layers whose stratification plane is parallel to the Earth's surface. The equivalence between a laminated medium and a TI medium holds when the dominant wavelength of the signal is long compared to the thickness of the layers (Backus, 1962; Carcione, 2007). Moreover, we obtain the energy balance, giving the energy scattering coefficients and the energy dissipated due to the interface specific viscosities.

2 Interface model and stress-strain relations

Let us consider a planar fracture separating two elastic and TI media. The non-ideal characteristics of the interface are modeled through the boundary conditions. The model proposed here is based on the discontinuity of the displacement and particle velocity fields across the interface. We consider the (x, z)-plane, and refer to the upper and lower media with the labels 1 and 2, respectively, with z increasing towards the lower medium (see Figure 1). Then, the boundary conditions for a wave impinging on the interface ($z = 0$) are

$$\begin{aligned} &\kappa_x[u_x] + \eta_x[v_x] = \sigma_{xz}, \\ &\kappa_z[u_z] + \eta_z[v_z] = \sigma_{zz}, \\ &[\sigma_{xz}] = 0, \\ &[\sigma_{zz}] = 0, \end{aligned} \tag{1}$$

where u_x and u_z are the displacement components, v_x and v_z are the particle-velocity components, σ_{xz} and σ_{zz} are the stress components, κ_x and κ_z are specific stiffnesses and η_x and η_z are specific viscosities. They have dimensions of stiffness and viscosity per unit length, respectively. Moreover, the brackets denote discontinuities across the interface, such that for a field variable ϕ, it is $[\phi] = (\phi)_2 - (\phi)_1$.

The model simulates the fracture by a zero width layer of distributed spring-dashpots. It can be shown that relaxation-like functions of Maxwell type govern the tangential and normal coupling properties of the crack. The interface exhibits time dependent mechanical properties through the relaxation functions, and, as in a viscoelastic material, this implies energy dissipation. The boundary conditions (1) are analized in appendix A by a plane wave analysis for normal incidence. A displacement discontinuity ($\kappa_z \neq 0$) yields a change of phase, while a discontinuity in the particle velocity ($\eta_z \neq 0$) implies an energy loss at the interface (Carcione, 1996, 1998, 2007); $\kappa_i = 0$, $i = 1(x), 3(z)$ gives the displacement discontinuity model and $\eta_i = 0$ gives the particle velocity discontinuity model. On the other hand, if $\eta_i \to \infty$, the model gives the ideal (welded) interface.

The characteristics of the medium are completed with the constitutive relations

$$\begin{aligned} \sigma_{xx} &= c_{11}\partial_x u_x + c_{13}\partial_z u_z, \\ \sigma_{zz} &= c_{13}\partial_x u_x + c_{33}\partial_z u_z, \\ \sigma_{xz} &= c_{55}(\partial_x u_z + \partial_z u_x) \end{aligned} \tag{2}$$

(Aki and Richards, 1980; Carcione, 2007), where c_{IJ} are the elastic constants of the background medium and ∂_i indicates partial derivative with respect to the spatial variable x_i.

3 Propagation characteristics in the anisotropic medium

A general plane-wave solution for the displacement field $\mathbf{u} = (u_x, u_z)$ is

$$\mathbf{u} = \mathbf{U} \exp\left[\mathrm{i}\omega(t - s_x x - s_z z)\right], \tag{3}$$

where s_z and s_z are the components of the slowness vector, $\mathbf{U}$ is a complex vector, t is the time variable, ω is the angular frequency and $\mathrm{i} = \sqrt{-1}$.

The dispersion relation of a TI medium is

$$(c_{11}s_x^2 + c_{55}s_z^2 - \rho)(c_{33}s_z^2 + c_{55}s_x^2 - \rho) - (c_{13} + c_{55})^2 s_x^2 s_z^2 = 0 \tag{4}$$

(e.g., Carcione, 2007), where ρ is the mass density. Equation (4) has two solutions corresponding to the quasi-compressional (qP) and quasi-shear (qS) waves.

Let us assume that the positive z-axis points downwards. In order to distinguish between down and up propagating waves, the slowness relation equation (4) is solved for s_3, given the horizontal slowness s_1. This yields

$$s_z = \pm\frac{1}{\sqrt{2}}\sqrt{K_1 \mp \mathrm{pv}\sqrt{K_1^2 - 4K_2K_3}}, \tag{5}$$

where

$$K_1 = \rho\left(\frac{1}{c_{55}} + \frac{1}{c_{33}}\right) + \frac{1}{c_{55}}\left[\frac{c_{13}}{c_{33}}(c_{13} + 2c_{55}) - c_{11}\right]s_x^2,$$

$$K_2 = \frac{1}{c_{33}}(c_{11}s_x^2 - \rho), \qquad K_3 = s_x^2 - \frac{\rho}{c_{55}},$$

and "pv" denotes the principal value. The signs in s_3 correspond to

$(+,-)$ downward propagating qP wave
$(+,+)$ downward propagating qS wave
$(-,-)$ upward propagating qP wave
$(-,+)$ upward propagating qS wave.

The plane-wave eigenvectors (polarizations) belonging to a particular eigenvalue can be obtained from the qP-qS Kelvin-Christoffel equation (Carcione, 2007). We obtain

$$\mathbf{U} = U_0 \begin{pmatrix} \beta \\ \xi \end{pmatrix}, \tag{6}$$

where U_0 is the plane-wave amplitude and

$$\begin{aligned} \beta &= \mathrm{pv}\sqrt{\frac{c_{55}s_x^2 + c_{33}s_z^2 - \rho}{c_{11}s_x^2 + c_{33}s_z^2 + c_{55}(s_x^2 + s_z^2) - 2\rho}}, \\ \xi &= \pm\mathrm{pv}\sqrt{\frac{c_{11}s_x^2 + c_{55}s_z^2 - \rho}{c_{11}s_x^2 + c_{33}s_z^2 + c_{55}(s_x^2 + s_z^2) - 2\rho}}, \end{aligned} \tag{7}$$

where the + and − signs correspond to the qP and qS waves, respectively. From equations (3) and (7), the particle-velocity field can be written as

$$\mathbf{v} = \mathrm{i}\omega\mathbf{u} = \mathrm{i}\omega U_0 \begin{pmatrix} \beta \\ \xi \end{pmatrix} \exp[\mathrm{i}\omega(t - s_x x - s_z z)]. \tag{8}$$

Substituting the plane wave (8) into the stress-strain relation (2) yields

$$\begin{aligned} \sigma_{xx} &= -\mathrm{i}\omega U_0 X, \\ \sigma_{zz} &= -\mathrm{i}\omega U_0 Z, \\ \sigma_{xz} &= -\mathrm{i}\omega U_0 W, \end{aligned} \tag{9}$$

where

$$\begin{aligned} X &= \beta c_{11}s_x + \xi c_{13}s_z, \\ Z &= \beta c_{13}s_x + \xi c_{33}s_z, \\ W &= c_{55}(\xi s_x + \beta s_z), \end{aligned} \tag{10}$$

The slowness components are given by

$$s_x = \frac{\sin\theta}{v(\theta)}, \qquad s_z = \frac{\cos\theta}{v(\theta)} \tag{11}$$

where θ is the phase propagation angle, measured with respect to the z-axis, and

$$v = \frac{1}{s} = \frac{1}{\sqrt{s_x^2 + s_z^2}} \tag{12}$$

is the phase velocity that can be obtained from the slowness relation (4). Hence, we have

$$\rho v^2 = \frac{1}{2}(c_{55} + c_{11}\sin^2\theta + c_{33}\cos^2\theta \pm C), \tag{13}$$

with

$$C = \sqrt{[(c_{33} - c_{55})\cos^2\theta - (c_{11} - c_{55})\sin^2\theta]^2 + (c_{13} + c_{55})^2\sin^2 2\theta}. \tag{14}$$

The + sign corresponds to the qP wave, and the − sign to the qS wave.

4 Reflection and transmission coefficients

The upper layer is denoted by the subscript 1 and the lower layer by the subscript 2. For clarity, the symbols P and S indicate the qP and qS waves, respectively. Moreover, the subscripts I, R and T denote the incident, reflected and transmitted waves. Using symmetry properties to define the polarization of the reflected waves, the displacements for a qP wave incident from above the interface are given by

$$\mathbf{u}_1 = \mathbf{u}_{P_I} + \mathbf{u}_{P_R} + \mathbf{u}_{S_R}, \tag{15}$$

$$\mathbf{u}_2 = \mathbf{u}_{P_T} + \mathbf{u}_{S_T}, \tag{16}$$

where

$$\mathbf{u}_{P_I} = (\beta_{P_1}, \xi_{P_1}) \exp\left[\mathrm{i}\omega(t - s_x x - s_{zP_1} z)\right], \tag{17}$$

$$\mathbf{u}_{P_R} = R_{\mathrm{PP}}(\beta_{P_1}, -\xi_{P_1}) \exp\left[\mathrm{i}\omega(t - s_x x + s_{zP_1} z)\right], \tag{18}$$

$$\mathbf{u}_{S_R} = R_{\mathrm{PS}}(\beta_{S_1}, -\xi_{S_1}) \exp\left[\mathrm{i}\omega(t - s_x x + s_{zS_1} z)\right], \tag{19}$$

$$\mathbf{u}_{P_T} = T_{\mathrm{PP}}(\beta_{P_2}, \xi_{P_2}) \exp\left[\mathrm{i}\omega(t - s_x x - s_{zP_2} z)\right], \tag{20}$$

$$\mathbf{u}_{S_T} = T_{\mathrm{PS}}(\beta_{S_2}, \xi_{S_2}) \exp\left[\mathrm{i}\omega(t - s_x x - s_{zS_2} z)\right]. \tag{21}$$

Application of Snell's law implies the continuity of the horizontal slowness s_x. The boundary conditions do not influence the emergence angles of the transmitted and reflected waves. The vertical slownesses s_{zP} and s_{zS}, as well as β_P, β_S, ξ_P and ξ_S, follow respectively the $(+,-)$ and $(+,+)$ sign sets given in equation (5). The choice $U_0 = 1$ implies no loss of generality.

The boundary conditions (1) are

$$[u_x] = c_x \sigma_{xz}, \quad [u_z] = c_z \sigma_{zz}, \quad [\sigma_{xz}] = 0, \quad [\sigma_{zz}] = 0, \tag{22}$$

where the superscripts indicate the medium, and

$$c_i = \frac{1}{\kappa_i + \mathrm{i}\omega\eta_i}, \quad i = 1(x), 3(z) \tag{23}$$

is a complex compliance per unit length characterizing the fracture.

Using the equations for the displacements and stresses, the boundary conditions generate the following matrix equation for the reflection and transmission coefficients:

$$\begin{pmatrix} \beta_{P_1} + \mathrm{i}\omega c_x W_{P_1} & \beta_{S_1} + \mathrm{i}\omega c_x W_{S_1} & -\beta_{P_2} & -\beta_{S_2} \\ \xi_{P_1} + \mathrm{i}\omega c_z Z_{P_1} & \xi_{S_1} + \mathrm{i}\omega c_z Z_{S_1} & \xi_{P_2} & \xi_{S_2} \\ Z_{P_1} & Z_{S_1} & -Z_{P_2} & -Z_{S_2} \\ W_{P_1} & W_{S_1} & W_{P_2} & W_{S_2} \end{pmatrix} \cdot \begin{pmatrix} R_{\mathrm{PP}} \\ R_{\mathrm{PS}} \\ T_{\mathrm{PP}} \\ T_{\mathrm{PS}} \end{pmatrix} = \begin{pmatrix} -\beta_{P_1} + \mathrm{i}\omega c_x W_{P_1} \\ \xi_{P_1} - \mathrm{i}\omega c_z Z_{P_1} \\ -Z_{P_1} \\ W_{P_1} \end{pmatrix}, \tag{24}$$

where W and Z are given by equations (10).

The steps to compute the reflection and transmission coefficients are the following:

1. The horizontal slowness s_x is the independent parameter. It is the same for all the waves (Snell's law). For an incident wave, the independent variable becomes the incidence angle θ, and s_x is obtained from equation (11).
2. Compute s_{zP_1}, s_{zS_1}, s_{zP_2} and s_{zS_2} from equation (5), where the first sign is positive. For an incident homogeneous wave, s_{zP_1} can be calculated either from equation (5) or from equation (11).

3. Compute β_{P_1}, β_{S_1}, β_{P_2}, β_{S_2}, ξ_{P_1}, ξ_{S_1}, ξ_{P_2} and ξ_{S_2} from equations (7).
4. Compute W_{P_1}, W_{S_1}, W_{P_2} and W_{S_2} and Z_{P_1}, Z_{S_1}, Z_{P_2} and Z_{S_2} from equations (10).
5. Compute the reflection and transmission coefficients by numerically solving equation (24).

Equation (24) gives the results of Carcione (1996) in the isotropic case, i.e., if $c_{33} = c_{11}$ and $c_{13} = c_{11} - 2c_{55}$. Carcione (1996) obtained the potential amplitude coefficients, which are related to the displacement amplitude coefficients by a conversion factor. In the case of isotropy and similar upper and lower media, the conversion factor from one type of coefficient to the other is 1 for PP coefficients and v_S/v_P for PS coefficients, where v_P and v_S denote the P- and S-wave velocities (Aki and Richards, 1980, p. 139).

When $c_x = c_z = 0$, equation (24) yield the reflection and transmission coefficients of a welded interface as in Wright (1987). At normal incidence and similar upper and lower media, we obtain

$$R_{PP} = \left(\mathrm{i}\frac{\omega_P}{\omega} - \frac{2\eta_z}{Z_P} - 1\right)^{-1} = \left(\frac{2\mathrm{i}c_z}{\omega Z_P} - 1\right)^{-1} \tag{25}$$

and

$$T_{PP} = 1 + R_{PP}, \tag{26}$$

(Carcione, 1998), where $Z_P = \sqrt{c_{33}/\rho}$ and $\omega_P = 2\kappa_z/Z_P$ is the characteristic frequency that defines the transition from an apparently perfect interface to the apparently decoupled one. If $\kappa_z = 0$, it is $\omega_P = 0$ and the particle velocity discontinuity model is obtained. In this case, the coefficients are frequency independent and there are no phase changes. On the other hand, when $\eta_z = 0$, the theory gives the displacement discontinuity model. A discontinuity in the particle velocity implies energy dissipation at the interface (Carcione, 1996, 1998). Moreover, if $\eta_z \to 0$ and $\kappa_z \to 0$, $R_{PP} \to 1$ and $T_{PP} \to 0$, and the free surface condition is obtained; when $\kappa_z \to \infty$ or $\eta_z \to \infty$, $R_{PP} \to 0$ and $T_{PP} \to 1$, giving the solution for a welded contact.

The coefficients are shown here as a function of the incidence ray angle ψ, which defines the direction of the energy-flux vector of the incidence wave. The ray angle can be obtained as

$$\tan\psi = \frac{\mathrm{Re}(\beta^*_{P_1} X_{P_1} + \xi^*_{P_1} W_{P_1})}{\mathrm{Re}(\beta^*_{P_1} W_{P_1} + \xi^*_{P_1} Z_{P_1})} \tag{27}$$

(Carcione, 2007), where "Re" takes real part and "$*$" denotes complex conjugate. Equation (27) holds for an incident viscoelastic medium. In this work, the medium is elastic and the real part and complex conjugate operation can be removed.

5 Energy balance and loss

In a completely welded interface, the normal component of the time-averaged energy flux is continuous across the plane separating the two media. This is a consequence of the boundary conditions that impose continuity of normal stress and particle velocity. The same property is valid if $\eta_x = \eta_z = 0$ (Carcione, 1996; Chiasri and Krebes, 2000). If the viscosities are non-zero, there is energy dissipation as shown in the following. Since the media are elastic, the interference fluxes between different waves vanish and

only the fluxes corresponding to each single beam need be considered (Carcione, 2007). Denoting by F the vertical component of the energy flux, we have

$$\begin{aligned}
-2F_{P_I} &= \mathrm{Re}(\sigma_{13P_I} v^*_{xP_I} + \sigma_{zzP_I} v^*_{zP_I}),\\
-2F_{P_R} &= \mathrm{Re}(\sigma_{13P_R} v^*_{xP_R} + \sigma_{zzP_R} v^*_{zP_R}),\\
-2F_{S_R} &= \mathrm{Re}(\sigma_{13S_R} v^*_{xS_R} + \sigma_{zzS_R} v^*_{zS_R}),\\
-2F_{P_T} &= \mathrm{Re}(\sigma_{13P_T} v^*_{xP_T} + \sigma_{zzP_T} v^*_{zP_T}),\\
-2F_{S_T} &= \mathrm{Re}(\sigma_{13S_T} v^*_{xS_T} + \sigma_{zzS_T} v^*_{zS_T})
\end{aligned} \tag{28}$$

(Carcione, 2007), where v_i are the components of the particle-velocity vector. As shown by Carcione (1997, 2007), further algebra implies that the fluxes given in the preceding equations are proportional to the real parts of

$$\begin{aligned}
F_{P_I} &\propto \beta^*_{P_1} W_{P_1} + \xi^*_{P_1} Z_{P_1},\\
F_{P_R} &\propto -(\beta^*_{P_1} W_{P_1} + \xi^*_{P_1} Z_{P_1}) |R_{\mathrm{PP}}|^2,\\
F_{S_R} &\propto -(\beta^*_{S_1} W_{S_1} + \xi^*_{S_1} Z_{S_1}) |R_{\mathrm{PS}}|^2,\\
F_{P_T} &\propto (\beta^*_{P_2} W_{P_2} + \xi^*_{P_2} Z_{P_2}) |T_{\mathrm{PP}}|^2,\\
F_{S_T} &\propto (\beta^*_{S_2} W_{S_2} + \xi^*_{S_2} Z_{S_2}) |T_{\mathrm{PS}}|^2,
\end{aligned} \tag{29}$$

where the proportionality factor is $\frac{1}{2}\omega^2$. We define the energy reflection and transmission coefficients as

$$ER_{\mathrm{PP}} = \sqrt{\frac{F_{P_R}}{F_{P_I}}}, \quad ER_{\mathrm{PS}} = \sqrt{\frac{F_{S_R}}{F_{P_I}}}, \quad ET_{\mathrm{PP}} = \sqrt{\frac{F_{P_T}}{F_{P_I}}}, \quad ET_{\mathrm{PS}} = \sqrt{\frac{F_{S_T}}{F_{P_I}}} \tag{30}$$

The energy loss at the interface is obtained by subtracting the energies of the reflected and transmitted waves from the energy of the incident wave. The normalized dissipated energy is

$$E_{\mathrm{loss}} = 1 - ER^2_{\mathrm{PP}} - ER^2_{\mathrm{PS}} - ET^2_{\mathrm{PP}} - ET^2_{\mathrm{PS}}. \tag{31}$$

At normal incidence we have

$$E_{\mathrm{loss}} = 1 - |R_{PP}|^2 - |T_{PP}|^2. \tag{32}$$

Substituting equations (25) and (26), the energy loss becomes

$$E_{\mathrm{loss}} = \frac{4\eta_z/Z_P}{(1 + 2\eta_z/Z_P)^2 + (\omega_P/\omega)^2}. \tag{33}$$

The maximum loss is obtained for

$$\eta_z = \frac{Z_P}{2}\sqrt{1 + \left(\frac{\omega_P}{\omega}\right)^2}. \tag{34}$$

6 Example

Seismic observations made in the vicinity of Dome C in East Antarctica show that the ice sheet there is TI with a vertical axis of symmetry (Blankenship and Bentley, 1987). We consider a planar fracture at 2.6 km depth in the ice sheet. The ice sheet at that depth has the properties

$$c_{11} = 16 \text{ GPa}, \quad c_{13} = 6.5 \text{ GPa}, \quad c_{33} = 14 \text{ GPa}, \quad c_{55} = 3 \text{ GPa}, \quad \rho = 920 \text{ kg/m}^3 \quad (35)$$

and

$$c_{11} = 18 \text{ GPa}, \quad c_{13} = 6.5 \text{ GPa}, \quad c_{33} = 16 \text{ GPa}, \quad c_{55} = 4 \text{ GPa}, \quad \rho = 940 \text{ kg/m}^3 \quad (36)$$

above and below the fracture, respectively (e.g., Carcione and Gei, 2003). See Thiel and Ostenso (1961) and Blankenship and Bentley (1987) for more information about the elasticity constants of the ice cap.

The fracture has the following parameters: $\kappa_x = \pi f_0 Z_S$, $\kappa_z = \pi f_0 Z_P$, $\eta_x = Z_S/50$ and $\eta_z = Z_P/50$, where $f_0 = 100$ Hz is a reference frequency and Z_P and Z_S are the impedances of the upper medium, related to the elastic constants c_{33} and c_{55}, respectively. The compliances values are $1/\kappa_x = 1.9 \times 10^{-9}$ m/Pa and $1/\kappa_x = 8.9 \times 10^{-10}$ m/Pa which are in agreement with values used in the literature (Chiasri and Krebes, 2000; Nakagawa and Myer, 2009). The complex compliances (23) represent viscoelastic Maxwell models (Carcione, 1996, 2007) and a quality factor can be defined as $Q_i = \kappa_i/(\omega\eta_i)$. In this case, $Q = 25 f_0/f$, which can be useful to quantify the energy loss at the interface. Figure 2 shows the absolute value (a) and phase (b) of the coefficients as a function of the ray angle for $f = \omega/(2\pi) = 100$ Hz ($Q_i = 25$), and Figure 3 shows the energy loss, indicating that 4 % of the energy is lost at the interface at $\psi = 0$. The amplitude peaks at nearly 75 degrees is a PP critical-angle effect, where maximum attenuation occurs. The absolute value of the coefficients (a) and normalized energy loss (b) for $f = 50$ Hz are displayed in Figure 4. In this case $Q_i = 50$, implying less energy dissipation (1.6 %). The reflection coefficient is lower than in the previous case ($f = 100$ Hz). Thus, the fracture acts as a low-pass filter for the transmitted P wave. In the absence of fracture ($\kappa_i \to \infty$, $\eta_i \to \infty$ or $c_x = c_z = 0$), the PP reflection coefficient is small at near and moderate angles (less than 0.04).

Figures 5, 6 and 7 shows the amplitude coefficients, the energy coefficients and the energy loss, respectively, for $f = 50$ Hz and an homogeneous medium whose properties are those of the upper medium. The critical-angle effect has disappeared. The dependence with frequency is displayed in Figure 8, where it can be seen that the reflection coefficient and dissipated energy decrease with decreasing frequency, confirming the low-pass filter property mentioned above. If $\omega \to \infty$ the energy loss (33) approaches the limiting value $4(\eta_z/Z_P)/(1 + 2\eta_z/Z_P)^2$.

7 Conclusions

A general linear model of an imperfect interface (e. g., a fracture) between two elastic media can be obtained by imposing boundary discontinuities to the displacement and particle velocity fields. The model can be expressed as displacement and particle-velocity discontinuities equivalent to a viscoelastic model. The P-S wave propagation problem requires two specific stiffnesses and two specific viscosities, which define the

properties of the non-ideal contact. Different choices of interface parameters give rise to the different conditions, from welded contact to stress-free boundary condition. The proposed model yields the scattering coefficients by a fracture embedded in transversely isotropic media. The fracture surface dissipates energy due to attenuation mechanisms present at the interface, as for instance, the interaction between a viscous fluid with the solid media. The fracture acts as a low-pass filter for the transmitted P wave and the reflection coefficient decreases at small and moderate ray angles.

References

1. Aki, K., and Richards, P. G., 1980, Quantitative seismology: Theory and methods, W. H. Freeman and Co.
2. Backus, G. E., 1962, Long-wave elastic anisotropy produced by horizontal layering, J. Geophys. Res., **67** , 4427-4440.
3. Blankenship, D. D., and Bentley, C. R., 1987, The crystalline fabric of polar ice sheets inferred from seismic anisotropy, The Physical Basis of Ice Sheet Modelling (Proceedings of the Vancouver Symposium, August 1987). IAHS Publ. no. 170.
4. Carcione, J. M., 1996, Elastodynamics of a non-ideal interface: Application to crack and fracture scattering, J. Geophys. Res., **101**, 28177-28188.
5. Carcione, J. M., 1997, Reflection and transmission of qP-qS plane waves at a plane boundary between viscoelastic transversely isotropic media, Geophys. J. Internat., **129**, 669-680.
6. Carcione, J. M., 1998, Scattering of elastic waves by a plane crack of finite width in a transversely isotropic medium, Int. J. Numer. Anal. Methods Geomech., **22**, 263-275.
7. Carcione, J. M., 2007, Wave fields in real media: Wave propagation in anisotropic, anelastic, porous and electromagnetic media, Handbook of Geophysical Exploration, vol. 38, Elsevier (2nd edition, revised and extended).
8. Carcione, J. M., and Gei, D., 2003, A seismic modeling study of a subglacial lake, Geophys. Prosp., **51**, 501-515.
9. Chiasri, S., and Krebes, E. S., 2000, Exact and approximate formulas for P -SV reflection and transmission coefficients for a nonwelded contact interface, J. Geophys. Res., **105**, 28045-28054.
10. Kundu, T., and Boström, A., 1992, Elastic wave scattering by a circular crack in a transversely isotropic solid, Wave Motion, **15**, 285-300.
11. Mroz, Z., and Giambianco, G., 1996, An interface model for analysis of deformation behaviour of discontinuities, Int. J. Num. Anal. Methods Geomech., **20**, 1-33.
12. Nagy, P. B., and Adler, L., 1990, New ultrasonic techniques to evaluate interfaces, in Elastic Waves and Ultrasonic Nondestructive Evaluations, edited by S. K. Datta *et al.* (Elsevier Sci. Pub., North-Holland), p. 229.
13. Nakagawa, S., and Myer, L. R., 2009, Fracture permeability and seismic wave scattering – Poroelastic linear-slip interface model for heterogeneous fractures, SEG Expanded Abstracts 28, 3461 (2009); doi:10.1190/1.3255581
14. Pyrak-Nolte, L. J., Myer, L. R., and Cook, N. G. W., 1990, Transmission of seismic waves across single natural fractures, J. Geophys. Res., **95**, 8617-8638.
15. Schoenberg, M., 1980, Elastic wave behavior across linear slip interfaces, J. Acous. Soc. Am., **68**, 1516-1521.
16. Thiel, E., and Ostenso, N. A., 1961, Seismic studies on antarctic ice shelves, Geophysics, **26**, 706-715.
17. Wright, J., 1987, The effects of transverse isotropy on reflection amplitude versus offset, Geophysics, **52**, 564-567.

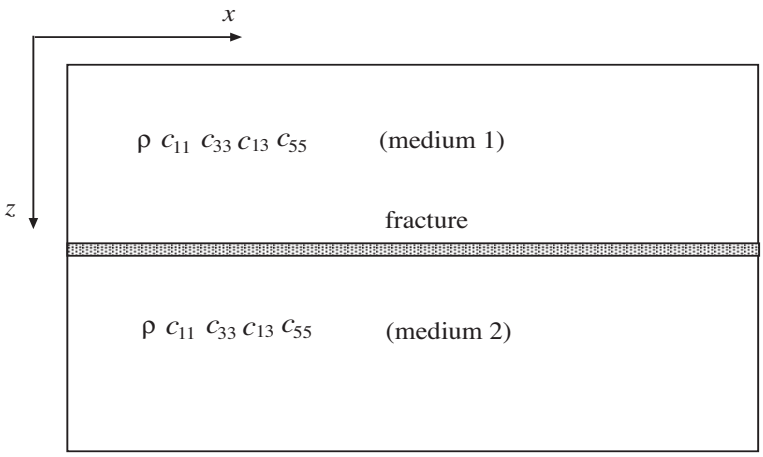

Fig. 1 Planar fracture embedded in transversely isotropic media of dissimilar density and elastic constants.

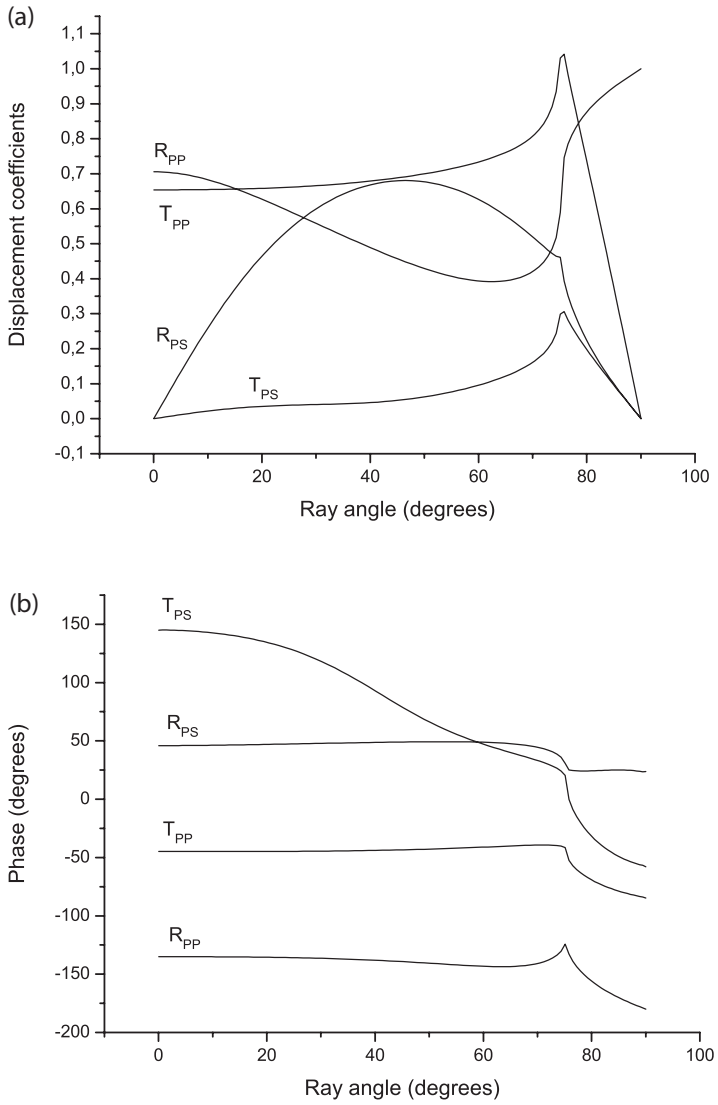

Fig. 2 Absolute value (a) and phase (b) of the scattering coefficients as a function of the ray angle for $f = 100$ Hz.

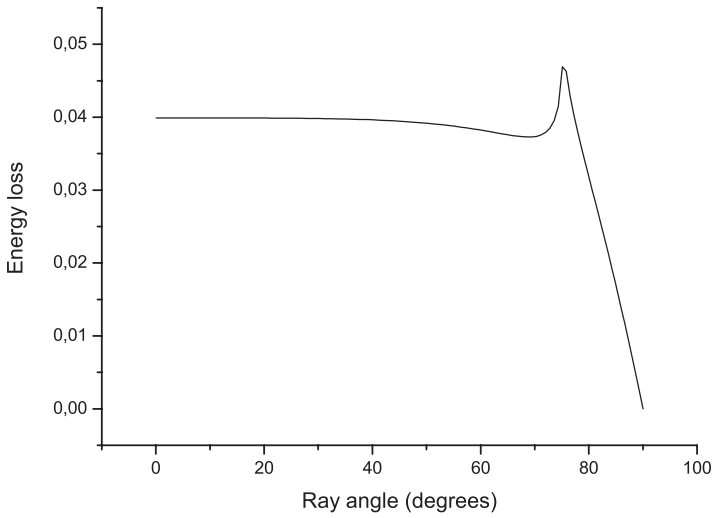

Fig. 3 Normalized energy loss as a function of the ray angle for $f = 100$ Hz.

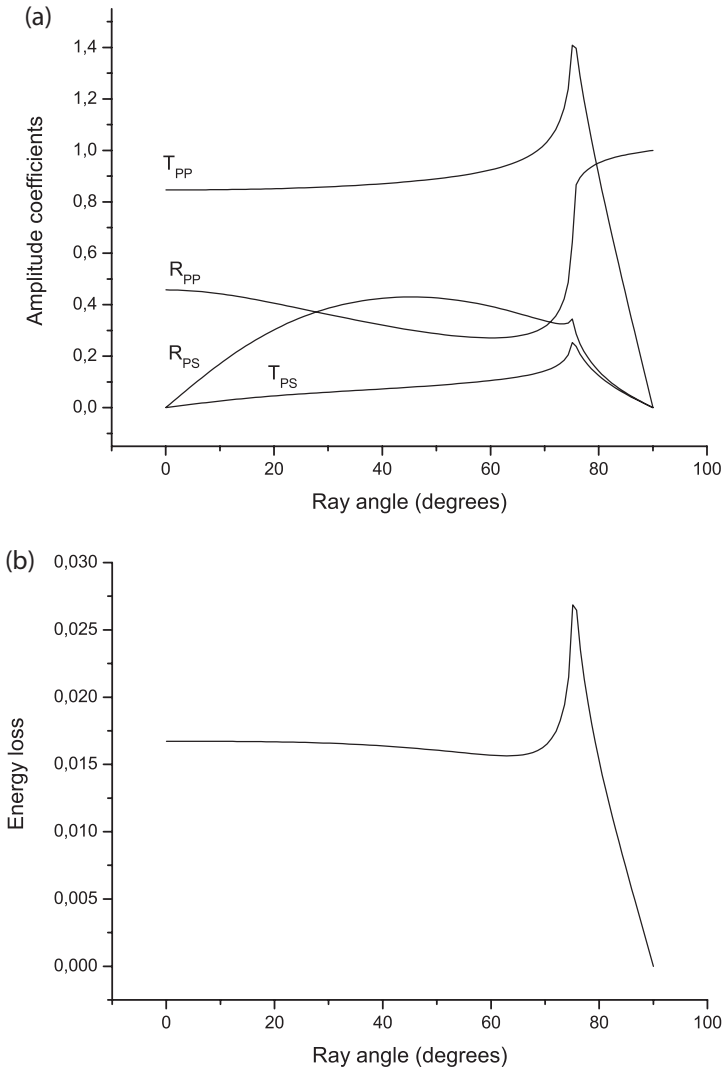

Fig. 4 Absolute value of the scattering coefficients (a) and normalized energy loss (b) as a function of the ray angle for $f = 50$ Hz.

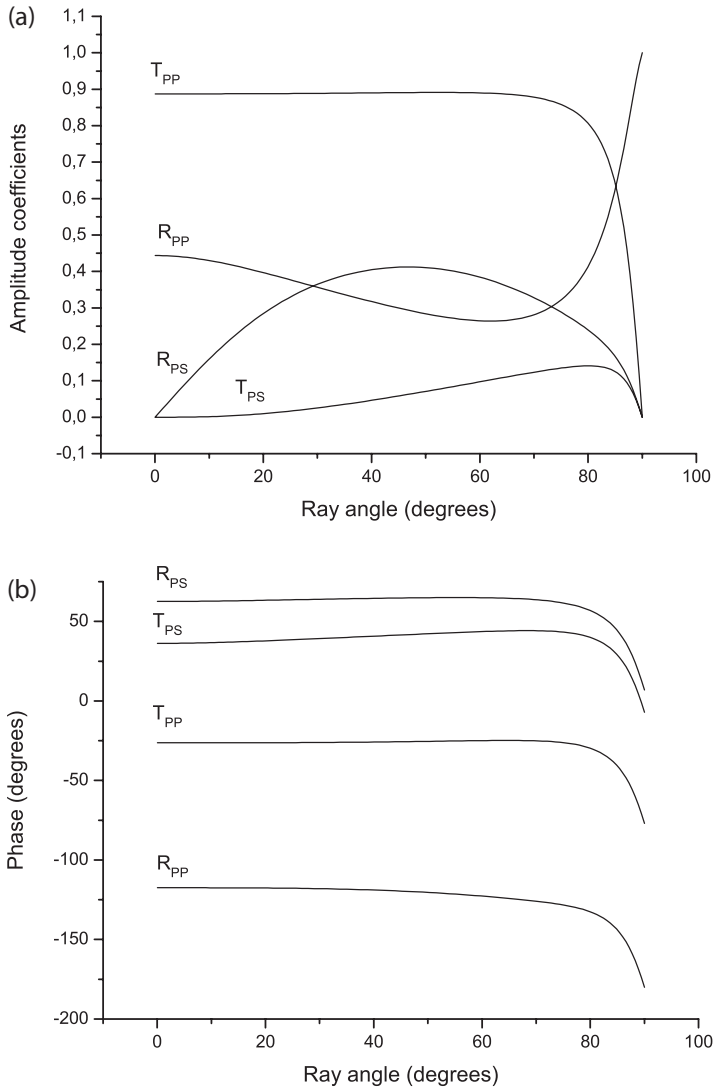

Fig. 5 Absolute value (a) and phase (b) of the scattering coefficients as a function of the ray angle for $f = 50$ Hz. The medium is homogeneous (the upper and lower media are the same).

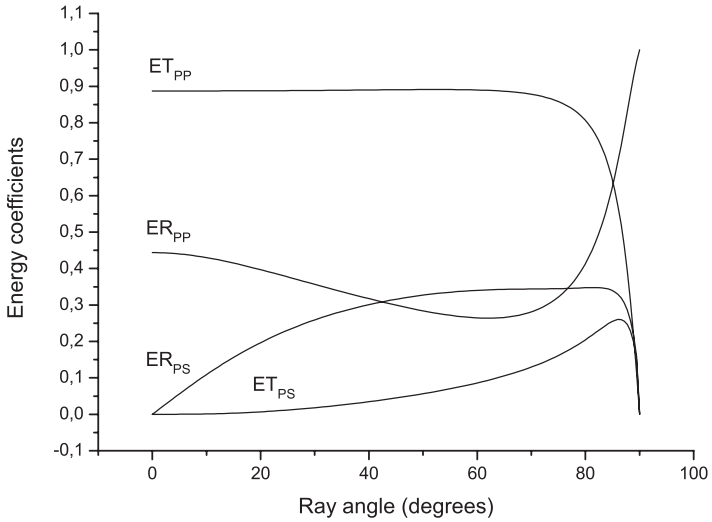

Fig. 6 Energy coefficients as a function of the ray angle for $f = 50$ Hz. The medium is homogeneous (the upper and lower media are the same).

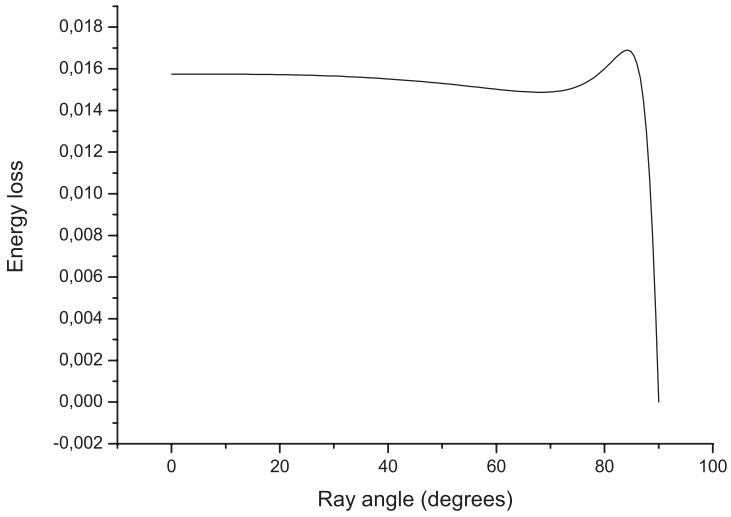

Fig. 7 Normalized energy loss as a function of the ray angle for $f = 50$ Hz. The medium is homogeneous (the upper and lower media are the same).

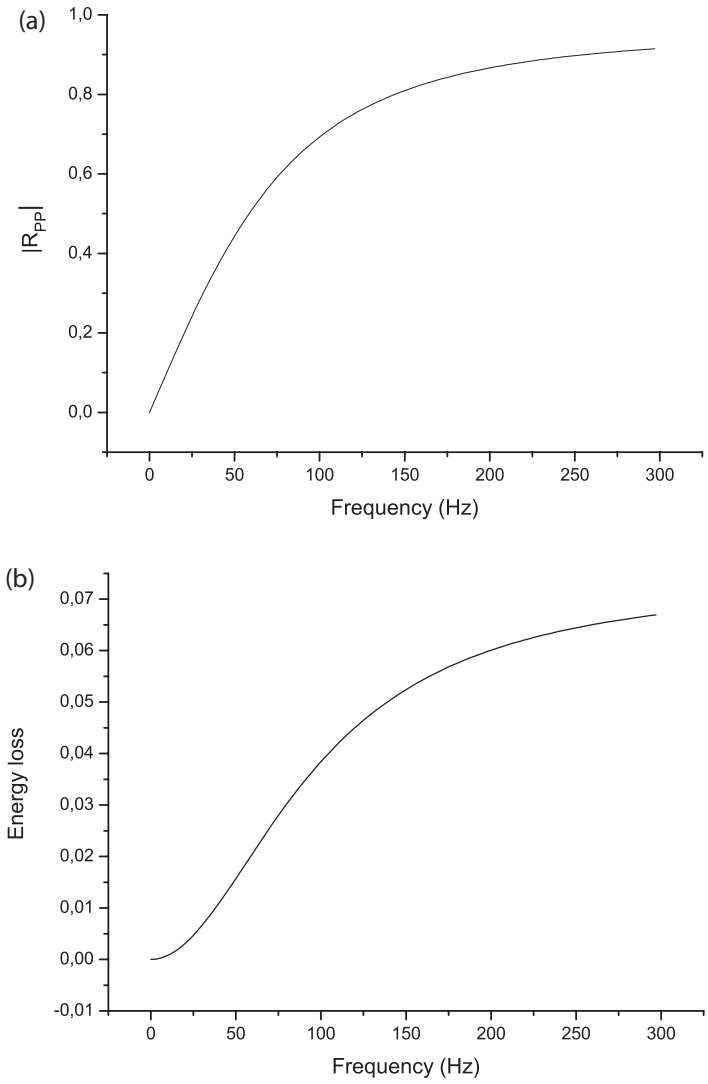

Fig. 8 Normal incidence reflection coefficient (a) and normalized energy loss (b) as a function of frequency. The medium is homogeneous (the upper and lower media are the same).